# Sliding Mode Controller Applied to Autonomous UAV Operation in Marine Small Cargo Transport

Guilherme F. Carvalho, Fabio A. A. Andrade, *Senior Member, IEEE*, Gabryel S. Ramos, Alessandro R. L. Zachi, Ana L. F. de Barros, and Milena F. Pinto, *Member, IEEE*

***Abstract*—Unmanned aerial vehicles (UAVs) have been used in different applications due to their flexibility in maneuvering and performing missions. However, they can face external disturbances, such as wind, which can cause physical instability of the platform. Usually, UAVs commonly use a classical PID controller due to their simple structure and less dependence on the model. However, this classical controller requires expertise from the operator to adjust the parameters when dealing with nonlinearities. Therefore, this work proposes the integration of a slide mode control (SMC) controller into a PX4 flight control unit (FCU) and combining it with computer vision techniques and sensor data fusion to enable autonomous UAV offshore cargo tasks for the Oil & Gas sector. The controller was evaluated in a software in the loop (SITL) simulation performed in the robot operating system (ROS), demonstrating its robustness and potential for small marine cargo transportation using UAVs.**

***Index Terms*—Flight control unit (FCU), offshore application, PX4, small cargo transport, SMC, unmanned aerial vehicle (UAV).**

## I. Introduction

UNMANNED aerial vehicles (UAVs) have been used in diverse applications. For instance, they are used in the inspection of large structures [1], [2], search and rescue activities [3], delivery goods [4], [5], security surveillance [6], [7], etc. UAVs present flexibility for maneuvering and performing tasks with short path length and maximum roll angle [8]. One of the main goals of the oil and gas industry is to improve the exploration process without losing manufacturing efficiency and quality [9]. Therefore, applying robots in this sector is a prominent solution to replace tasks that can be unsafe for humans or cause worker depletion [10].

There is a growing interest in researchers that publishes works applying UAVs to automate tasks in the Offshore industry, such as [11] and [12]. According to [13], UAVs offer faster, safer, and more cost-efficient ways of mass data collection, which can directly impact the reduced costs in a few applications.

For instance, Ramos et al. [14] applied an autonomous UAV to deliver a message cable from the shuttle tanker to the floating, production, storage, and offloading (FPSO) unit. Dai et al. [15] investigated the application of UAVs for data offloading for smart containers in offshore maritime communications. The UAV relays on a node between smart containers and an onshore base station in their application. For a complete overview of UAVs remote sensing in the oil and gas industry, the authors refer to [16].

Note that the selection of UAVs depends on different factors, including the coverage area, distance from the base station, flight duration, and the sensors aboard the UAV [16]. Cameras, by far, are the most widely used sensors aboard UAVs [17]. Using computer vision techniques and a self-controlling function to fly in an unstructured environment to perform the autonomous survey makes it possible to use UAV versatility to improve and substitute the riskier jobs. Such examples are the inspection of power and transmission lines [18], dams [19], or buildings [20]. Other tasks that autonomous UAVs can perform are transporting materials or equipment between predefined locations, like offshore landing platforms on ships and support vessels nearby. In this case, computational vision techniques could be used to identify landing zones [21].

For autonomous or semiautonomous operations, the UAV should also be capable of performing these missions stably. The control design for quadrotor UAVs has two main challenges. The first challenge regards the fact that the quadrotor is a multiple-input–multiple-output (MIMO) unstable nonlinear systems, presenting four actuators and six degrees of freedom (DOFs). The second issue is that this kind of robot faces different difficulties, such as external and internal disturbances, uncertainty in the model, and parametric perturbations [22]. In this sense, many attempts from the literature suggested the use of different robust approaches to improve the reliability of the UAV controller to compensate for the effects of the external disturbances [10], [23], [24], [25], such as feedback

Manuscript received 3 January 2023; revised 31 March 2023 and 19 June 2023; accepted 9 July 2023. Date of publication 18 July 2023; date of current version 20 November 2023. *(Corresponding author: Fabio A. A. Andrade.)*

Guilherme F. Carvalho, Gabryel S. Ramos, Alessandro R. L. Zachi, Ana L. F. de Barros, and Milena F. Pinto are with the Electrical Engineering Post-Graduation Department, Federal Center for Technological Education of Rio de Janeiro, Rio de Janeiro 20271-110, Brazil (e-mail: gruilhermefercar@gmail.com; gabryelsr@gmail.com; alessandro.zachi@cefet-rj.br; ana.barros@cefet-rj.br; milena.pinto@cefet-rj.br).

Fabio A. A. Andrade is with the Department of Microsystems, University of South-Eastern Norway, 3184 Borre, Norway, and also with the Drones and Autonomous Systems Research Group, NORCE Norwegian Research Centre, 5838 Bergen, Norway (e-mail: fabio@ieee.org).

Digital Object Identifier 10.1109/JMASS.2023.3296433

linearization [26], [27], dynamic inversion [28], [29], sliding mode control [30], [31], backstepping [32], [33], and others.

The flight control unit (FCU) is the main component in this entire hardware setup, known as the brain of this underactuated quadcopter. The controller's firmware has many parts working in parallel that are responsible for maintaining the drone's stability and desired position. Citing just a few parts, we have the outermost position controller, the speed controller, the tilt controller, and the angular acceleration controller, which are responsible for the main cascade control loop, which is best explained in [34]. In addition, we also have the motor mixer, which is responsible for distributing the output values to the drone actuators so that the propellers behave correctly. Another important component of the control cascade is the world-to-body conversion module that translates the coordinates passed with the global frame reference to the UAV reference. The most difficult part when modifying this controller is understanding how all the modules communicate and where each modification should be done to achieve the desired result or behavior. The FCU is the piece of hardware that encapsulates all the sensors and processing cores that the control software will use to generate the desired outputs.

The main contribution of this work is developing and implementing an SMC controller in a PX4 FCU software for quadrotor UAV for position control. Besides, this work also proposed the use of this SMC-based controller along with a computer vision technique to apply an autonomous UAV in an offshore cargo transport task in the Oil and Gas scenario. The work also considers a classical PID controller for comparison purposes. The main contributions can be summarized as follows.

1) Implementation of an SMC controller in a PX4 FCU software for quadrotor UAV for position control.
2) Development of an SMC-based and Computer Vision technique that enables the UAV to fly autonomously between vessels to deliver materials.
3) Experimental tests are carried out in a realistic simulation environment by using the robot operating system (ROS)/Gazebo platforms to verify the performances of the proposed methodology.

As mentioned, Ramos et al. [12] proposed a framework that fuses flight data information from UAV sensors and an object detection algorithm based on YOLOv3 to deploy the vehicle from an oil rig and safely reach a shuttle tanker vessel nearby. The context of such a proposal is to assist the mooring process in offloading operations. A thin messenger line must be carried from the vessel to the production facility so it can be tied. Besides being complete, the work fails to analyze stability and environmental effects on the UAV's flight. It proposes a solution for this issue, focusing on developing and simulating the hybrid approach. The present work takes a step ahead, covering control solutions to deal with wind and flight instabilities during this operation using the SMC controller.

The remainder of this article is organized as follows. Section II gives the necessary background for cargo transport in the Oil and Gas industry. Also, this section presents related works in the employment of SMC controllers for quadrotor UAV controlling. Section III shows the mathematical foundations for the control strategy and its implementation in a real FCU. Section V presents the results and discussions. The concluding remarks and ideas for future works are given in Section VI.

## II. Background and Related Works

### A. Sliding Mode Controller

The external disturbances can cause physical instability of the UAV's platform. UAVs commonly use a classical PID controller with a simple structure, good stability, and less dependence on the exact system model [10]. However, the PID process of adjusting the parameters requires expertise, especially when dealing with nonlinearities. For instance, the authors of work [35] proposed using a self-tuned PID control method to handle external disturbances in a quadrotor UAV. Carvalho et al. [36] proposed using a PID and Fuzzy Logic hybrid controller. The fuzzy logic was used to schedule the PID controller. Another kind of controller for UAV stabilization was used in [37]. In their work, the authors proposed a sliding mode control based on neural networks for the attitude and altitude system of quadcopters under external disturbances. The controller evaluation was performed by numerical simulation.

The sliding mode control (SMC) arises as a robust control design to deal with uncertain conditions for complex high-order nonlinear systems [38], [39], [40], [41], [42], [43].

The main advantage of the SMC technique is its low sensitivity to disturbances and system parameter variations, being widely employed for trajectory tracking control algorithms [44]. Mofid and Mobayen [41] proposed using an adaptive sliding mode control strategy to stabilize quadrotor UAVs that present parametric uncertainties. Another use of the SMC strategy is proposed in [42]. In their work, the authors proposed using a sliding-mode-observer-based equivalent-input-disturbance approach to handle the disturbance suppression of quadrotors. Both works evaluated their results using numerical simulation analysis.

In SMC design formalism, the commonly chosen sliding surface $s(X)$ is a function of the state variables $X = [x, \dot{x}, \ldots, x^{(n-1)}]^T$, namely

$$s(X) = x^{(n)} + \lambda_{n-1}x^{(n-1)} + \cdots + \lambda_1\dot{x} + \lambda_0 x = 0. \tag{1}$$

The surface in (1) defines a region in state space where the control structure changes will be applied. Once the state trajectories reach this surface, it remains invariant, that is, $s(X) = 0$, and then the closed-loop system exhibits a desirable behavior which is defined by the coefficients $\lambda_i$ $(i = 1, \ldots, n-1)$ in (1). In the following, we briefly show that such behavior can be performed via a switched-type control law in the form:

$$u \coloneqq -\rho \ \text{sign}[s(X)] \tag{2}$$

with

$$\rho > 0 \in \Re, \qquad \text{sign}[s(X)] = \begin{cases} -1, & s(X) < 0 \\ 0, & s(X) = 0 \\ 1, & s(X) > 0. \end{cases} \tag{3}$$

Let us consider, for example, a class of second-order systems in the format

$$\ddot{x} = u + g(t) \tag{4}$$

in which $x \in \Re$ is the system output, $u \in \Re$ is the system control input, and $g(t) \in \Re$ is a function that represents some disturbance term. Here, the main assumptions are as follows.

(A1) A real upper bound constant $\rho > 0$ is known for $|g(t)|$, i. e., $\rho > |g(t)|$.

(A2) The state variables $\dot{x}$ and $x$ are available.

If the control input is chosen as

$$u = -\lambda\dot{x} - \rho \ \text{sign}(s), \quad \lambda > 0 \tag{5}$$

$$s = \dot{x} + \lambda x \tag{6}$$

then, the closed-loop system becomes

$$\ddot{x} + \lambda\dot{x} = \dot{s} = -\rho \ \text{sign}(s) + g(t). \tag{7}$$

For analyzing the stability of the previous closed-loop system, let us choose the following Lyapunov function candidate:

$$V(s) = \frac{1}{2}s^2. \tag{8}$$

The time derivative of (8) over the trajectories of (7) is given by

$$\dot{V}(s) = s\,\dot{s} = -\rho|s| + sg(t) = -|s|\left[\rho + g(t)\ \text{sign}(s)\right]. \tag{9}$$

Since the magnitude of the term "$g(t)$ sign$(s)$" cannot overcome the magnitude of $\rho$, as assumed by Assumption (A1), then we conclude that $\dot{V} < 0$. The last condition guarantees that $s \to 0$ for some finite time $t = t_f$. Thus, after the system trajectories (4) reach the sliding surface $s = 0$ (6) for $t \geq t_f$, one has that

$$\dot{x} + \lambda x = 0 \tag{10}$$

which does imply that $x \to 0$ exponentially fast.

As the aforementioned structural change occurs via a switched-type control law, the abrupt changes that can cause unwanted oscillations are known as *chattering* [45]. This technique's known disadvantage can become accentuated if there are response delays between the actuator and the controller [46]. A well-known fact in the literature is that the chattering phenomenon can be avoided by adopting a smooth control law instead of the switching one in (5). However, with such smoothing, the closed-loop system loses the sliding property. In this case, the trajectories of the system do not converge to the surface $s = 0$ but lie in a residual region around it that is denoted by a *boundary layer* [45]. For instance, if a smooth control law

$$u = -\lambda\dot{x} - \rho \ \tanh(s) \tag{11}$$

is used instead of its switched-type version in (5), then the Lyapunov function derivative of (9) would have the following format:

$$\dot{V}(s) = s\,\dot{s} = -|s|\left[\rho|\tanh(s)| + g(t)\ \text{sign}(s)\right]. \tag{12}$$

One can note that by adopting such a smoothing approach, the magnitude of the term "$\rho|\tanh(s)|$" decreases with $s$ and cannot always overcome the magnitude of the disturbance term "$g(t)$ sign$(s)$" as before. In this case, $\dot{V}(s) < 0$ can be guaranteed only outside a certain region around the origin defined by

$$|\rho \ \tanh(s)| > |g(t)| \tag{13}$$

which, as mentioned, is well known by the boundary layer region [45]. In the following, we apply the SMC to control a UAV for the cargo transporting problem.

### B. Cargo Transport in Marine Offshore Scenario

Currently, the use of UAVs in general transport applications is consolidated and well documented, as established in [47]. The operations may vary from parcel delivery to human transportation [48], enhancing the logistic chain efficiency, reducing costs compared to conventional delivery options, and reducing environmental damage by eliminating the emission of polluting gases. The study of UAV controllers and aircraft designs reduced the vehicles' manufacturing costs and advanced the technology for more audacious applications, such as human organ and medicine transport in emergencies [49].

The naval industry has used the robotic framework in several applications since the 70's decade, mainly in the form of remotely operated vehicles (ROVs) for underwater inspections [50]. Recently, the versatility of UAVs and aerial robotics systems caught the attention of the naval industry for small parcels transportation [9], naval operations assistance, such as in ship maneuver on ports [51] and offloading hose connection [12], an inspection of naval structures [52], marine search and rescue [53], among others. One particular application drawing attention in this sector is cargo transport. Traditional marine logistics is restricted to transshipment by boats, vessels, and helicopters.

Usually, the aerial alternative is used for small cargo. However, it presents some restrictions for transportation and navigation [54]. For instance, there is a restriction to transporting some packages, such as inflammable petrochemical samples, cutting or piercing tools, explosive components (i.e., batteries), etc. Using boats for transport demands the manipulation of cargo by cranes (even when it is lightweight) or launching the cargo in water (for example, in offloading operation mooring and connection stages). In this sense, UAV represents an attractive alternative for small cargo transport. It could easily replace the conventional means for small cargo transport between near naval structures, eliminating traditional restrictions while improving efficiency [55], [56].

In the context of our research work, an autonomous UAV is applied to an offshore cargo task for the Oil and Gas sector. An SMC controller is implemented in the PX4 flight control software for the quadrotor to perform position control. The navigation process is based on the work of our group lab article [12]. They used a hybrid approach based on deep learning and sensor fusion for the path planning of autonomous UAVs. Fig. 1 presents the operation in marine small cargo transport performed by a UAV between a shuttle tanker and an FPSO.

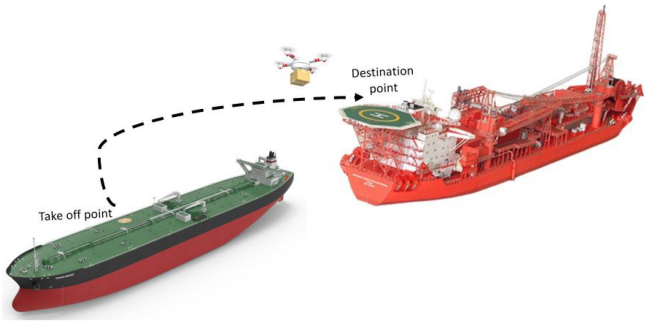


Fig. 1. Cargo transport scheme.

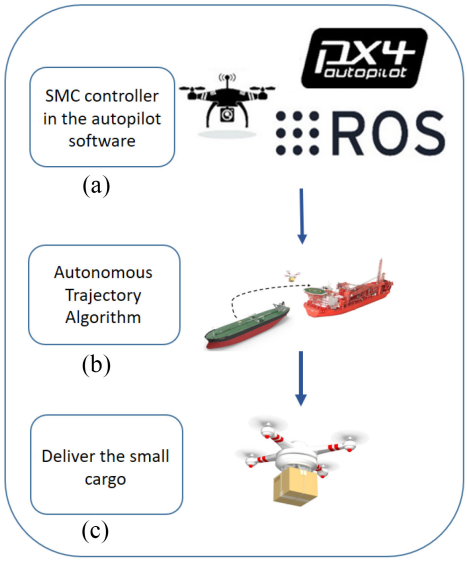


Fig. 2. Overview flowchart. (a) SMC controller is implemented to substitute the PID controller in the FCU due to the wind disturbances of the marine operation. (b) Autonomous trajectory method is used to autonomously guide the UAV to the delivery point in the destination vessel. (c) When arriving at the delivery point, the UAV delivers the small cargo.

This is a complex and difficult marine operation due to the windy disturbance and difficulty of reaching a safe place to land or drop the cargo.

## III. Proposed Methodology

This research aims to deliver a small cargo in a marine operation from one vessel platform to another. As stated before, autonomous navigation is derived from previous work from our group research and is available at [12]. Therefore, this work only focuses on the control strategy to perform the cargo transport in this scenario with stability and safety. For this reason, we implemented an SMC controller in a PX4 FCU software for the position controller. This controller will be the base for data acquisition and actuator control. We modified the current PID control strategy as an innovative approach and inserted the SMC logic inside the internal rate control module. Fig. 2 presents the process in a simplified way.

### A. Quadrotor Model

When deriving the dynamic model, it is important to consider the quadrotor as a nonlinear unstable system that

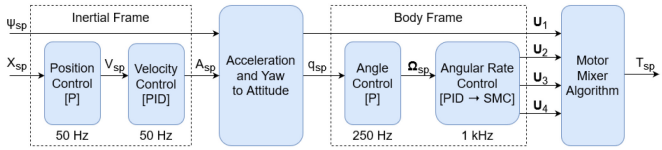


Fig. 3. Quadrotor UAV architecture.

TABLE I
Variable Descriptions Used in the Set of Quadrotor Equations

| Variable | Description |
|---|---|
| $\phi$, $\theta$ and $\psi$ | Euler angles *roll*, *pitch* and *yaw* |
| $Ixx$, $Iyy$, $Izz(kgm^2)$ | Moment of inertia about Earth frame |
| $m(kg)$ | Total vehicle mass |
| $l(m)$ | Quadcopter arm length |
| $b(Ns^2)$ | Impulse coefficient |
| $d(Nms^2)$ | Drag coefficient |
| $Jr(kgm^2)$ | Rotor moment of inertia |
| $\Omega_r$ | Engines residual angular speed |
| $\xi_{(\phi,\theta,\psi,h)}$ | Euler angles disturbances |
| $U_1$ | Thrust equivalence force |
| $U_2$ | Rotational force on roll axis |
| $U_3$ | Rotational force on pitch axis |
| $U_4$ | Rotational force on yaw axis |

comprises four actuators whose thrust is treated as an input to the entire system. Besides, this work considers a quadrotor body frame as a rigid and symmetrical structure.

Fig. 3 presents a widespread quadrotor control architecture. Article [34] could better describe this architecture. Our approach, as described before, was to modify the controller logic on the "Angular Rate Control" block in order to implement an SMC-based controller in place of the current PID controller.

Table I presents the variables descriptions used in the set of equations for modeling the quadrotor.

The angles $\phi$, $\theta$, and $\psi$ are used as the inputs of the forward kinematics equation computing the conversion matrix of the world to the body frame. Note that based on the estimated values of the Euler angles and velocity at each moment, it is possible to estimate the UAV position as shown in (14) where $\cos(\psi)$ is shown as $C_\psi$ and $\sin(\theta)$ is $S_\theta$

$$R_{(\phi,\theta,\psi)} = \begin{bmatrix} C_\phi C_\theta C_\psi - S_\phi S_\psi & - C_\phi C_\theta C_\psi - S_\phi S_\psi & C_\phi S_\theta \\ S_\phi C_\theta C_\psi + C_\phi S_\psi & - C_\phi C_\theta C_\psi + S_\phi S_\psi & S_\phi S_\theta \\ -S_\theta S_\psi & S_\theta S_\psi & C_\theta \end{bmatrix}. \quad (14)$$

Equation (15) presents the UAV body frame axes mathematical model. For this type of model limitations and characteristics, the authors refer to [57] and [36]. Besides, an appropriate and nearer dynamical model for quadrotor can be seen at [58], [59]. Equation (15) has the following auxiliary variables $\Delta = \cos(\phi)\sin(\theta)\cos(\psi)$ and $\Gamma = \cos(\phi)\sin(\theta)\sin(\psi)$:

$$\begin{bmatrix} \ddot{\phi} \\ \ddot{\theta} \\ \ddot{\psi} \\ \ddot{z} \\ \ddot{x} \\ \ddot{y} \end{bmatrix} = \begin{bmatrix} \frac{I_{yy}-I_{zz}}{I_{zz}}\dot{\theta}\dot{\psi} + \theta\frac{J_r}{I_{xx}}\Omega_r + \frac{l}{I_{xx}}U_2 \\ \frac{I_{zz}-I_{zz}}{I_{yy}}\dot{\phi}\dot{\psi} + \phi\frac{J_r}{I_{yy}}\Omega_r + \frac{l}{I_{yy}}U_3 \\ \frac{I_{xx}-I_{yy}}{I_{zz}}\dot{\theta}\dot{\phi} + \frac{l}{I_{zz}}U_4 \\ g - \frac{\cos(\phi)\cos(\theta)U_1}{m} \\ \frac{U_1}{m}(\Delta + \sin(\phi)\sin(\psi)) \\ \frac{U_1}{m}(\Gamma + \sin(\phi)\cos(\psi)) \end{bmatrix} = \begin{bmatrix} \xi_\phi(t) \\ \xi_\theta(t) \\ \xi_\psi(t) \\ \xi_h(t) \\ 0 \\ 0 \end{bmatrix} \quad (15)$$

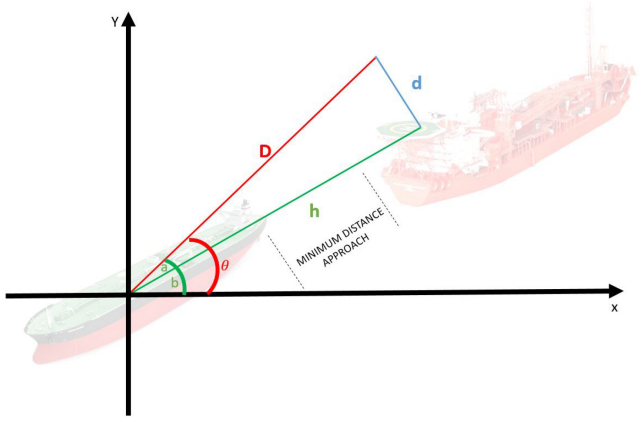


Fig. 4. Linear trajectory.

where the thrust and the actuation torque for the roll, pitch, and yaw movements are $U_i|(i = 1, \ldots, 4)$ variables [36].

By using the motor mixing algorithm, it is possible to combine these variables and analyze the $U_i$ inputs related to the angular speeds of the rotors $\Omega_{(1,2,3,4)}$

$$\begin{bmatrix} U_1 \\ U_2 \\ U_3 \\ U_4 \\ \Omega_r \end{bmatrix} = \begin{bmatrix} b\left(\Omega_1^2 + \Omega_2^2 + \Omega_3^2 + \Omega_4^2\right) \\ b\left(-\Omega_2^2 + \Omega_4^2\right) \\ b\left(\Omega_1^2 - \Omega_3^2\right) \\ d\left(-\Omega_1^2 + \Omega_2^2 - \Omega_3^2 + \Omega_4^2\right) \\ -\Omega_1 + \Omega_2 - \Omega_3 + \Omega_4 \end{bmatrix}. \tag{16}$$

## B. Autonomous Trajectory

For the autonomous trajectory, the authors refer to a previous work of our group lab [12]. In this scheme, the location of the delivery point is configured in the UAV's offboard through GPS coordination. Besides, the operator informs the desired distance between the ship and the vehicle for security purposes. The trajectory calculation starts from reading the coordinates of the takeoff point through GPS, making this the origin of a 3-D Cartesian system ($x$-axis oriented toward the east, $y$-axis oriented toward magnetic north, and $z$-axis being the altitude). The designed trajectory is presented in Fig. 4. Note that this straight line is to avoid gas escapes points and classified areas around the vessels.

Given the destination and the takeoff coordinates, it is possible to calculate the distance $D$ between the takeoff point, and the final point of the first step of the trajectory based on [60], and shown in

$$D = R \cdot \arccos\left(\sin(\text{Lat}_i) \cdot \sin\left(\text{Lat}_f\right) + \cos(\text{Lat}_i) \cdot \cos\left(\text{Lat}_f\right) \cdot \cos\left(\text{Lon}_i - \text{Lon}_f\right)\right) \tag{17}$$

where the parameters Lat and Lon represent the GPS coordinates (in radians) and the notations "$i$" and "$f$" are the takeoff location and destination point. $R$ symbolizes the Earth's radius, admitted as $6.373 \times 10^6$ m. Equation (18) gives the destination azimuthal direction $\theta$ from the takeoff point

$$\theta = \arctan \cdot \frac{\Delta_{(\text{Lon})}}{\Delta_{(\phi)}} \tag{18}$$

where

$$\Delta\phi = \log\left[\frac{\tan\left(\frac{\text{Lat}_f}{2} + \frac{\pi}{4}\right)}{\frac{\text{Lat}_i}{2} + \frac{\pi}{4}}\right] \tag{19}$$

$$\Delta\text{lon} = |\text{Lon}_i - \text{Lon}_f|. \tag{20}$$

Note that the destination point of the vessel is not where the UAV delivers the cargo but a location distant from the delivery point by a distance $d$. The control node receives this information and measures the UAV's distance from the target. The trajectory calculation publishes this route to the controller with the points $(x, y)$, the flight height at each point $(z)$, and the robot's orientation (yaw) at each point.

To approach the destination, it is implemented a hybrid methodology in which the controller detects the vessel and its generic regions (bow, mid-ship, and stern) by a convolutional neural network for object detection and fuses it with position and attitude data using an extended Kalman filter (EKF) to navigate toward the delivery point, anticipating any drifting caused by wind or yaw controller error while maintaining a safe approaching speed to the destiny, as detailed in [12].

## C. Control Design and Implementation in PX4

The PX4 firmware is used as a code base to implement and test the SMC controller in a quadrotor UAV. The purpose is to modify the part of the code responsible for controlling the UAV angular rate, that is, the most internal part of the cascading controller, as shown in Fig. 3.

The idea for this case is to replace the angular rate controller, which is the lowest level controller in the cascade, by the first order SMC with a relative degree of 2 represented by (21) in which $\kappa > 0 \in \Re$ is the modulation constant, $\alpha,\ \beta,\ \gamma > 0 \in \Re$ are design parameters, and $\sigma \in \Re$ defines the sliding surface. In (22), the $\tanh(\cdot)$ function is adopted in the following for smoothness purposes. The objective is to reduce the chattering phenomenon in the control command to be applied to the actuators. Since SMC is applied in the subsystems of (15)–(16), to represent them in a standardized way, we define generalized control and output error signals $u$ and $e$, respectively, as

$$u = \kappa \tanh(\sigma) \tag{21}$$

$$\sigma = \alpha e + \beta \int e\, dt + \gamma \dot{e}. \tag{22}$$

In (21) and (22), $\sigma$ stands for the generalized sliding surface that is computed for every subsystem in (15) and (16). It is important to mention that, in practice, the control signals generated by (22) are transformed to $U_2$, $U_3$, and $U_4$ of (15) and (16) which are torque commands for roll, pitch, and yaw axis, respectively. Similarly to other SMC controllers, the proposed one in (21) and (22) use a higher order sliding surface provided that the velocity information is available from the sensor's telemetry. This controller is implemented at the top of the PX4 firmware as a base for data acquisition and actuator control. A fork of the official repository was made. By following the provided documentation [61], the current cascade PID control was modified to insert the SMC logic

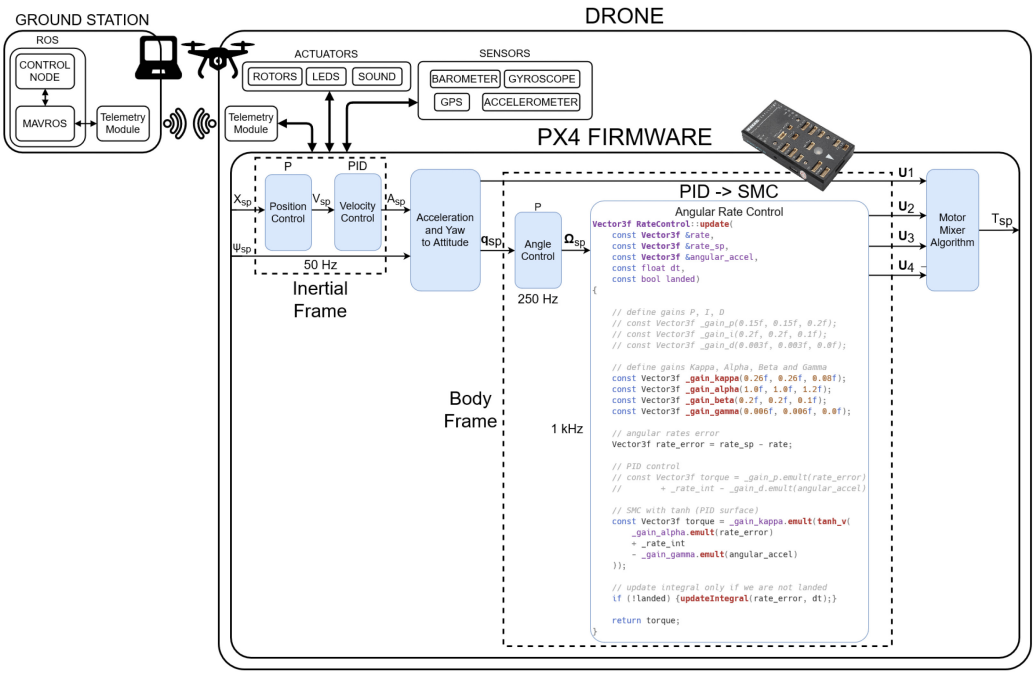


Fig. 5. SMC implemented in the PX4 Firmware.

inside the internal rate control module. All the documentation on how to run this simulation yourself and the source code change can be found at piradata-WPG (python module for tests) and piradata-Firmware (Modified PX4 Firmware, mainly file RateControl.cpp on directive RateControl::update). Fig. 5 presents a general idea of this work proposition.

## IV. Stability and Convergence Analysis

Let us define the vector of state variables as in (15), namely, $\mathcal{X} = [\dot{\phi},\ \dot{\theta},\ \dot{\psi},\ \phi,\ \theta,\ \psi,\ z,\ x,\ y]^T$. In this way, the expressions of (15) can be rewritten as

$$\ddot{\phi} = f_\phi(\mathcal{X}) + k_\phi u_2, \quad \ddot{\theta} = f_\theta(\mathcal{X}) + k_\theta u_3 \tag{23}$$

$$\ddot{\psi} = f_\psi(\mathcal{X}) + k_\psi u_4, \quad \ddot{x} = f_x(\mathcal{X})u_1 \tag{24}$$

$$\ddot{y} = f_y(\mathcal{X})u_1, \qquad \ddot{z} = g - f_z(\mathcal{X})u_1 \tag{25}$$

in which $f_\eta(\mathcal{X})$ stand for the nonlinear parts, $k_\eta$ are constants or nonlinear functions, $u_\eta = U_\eta$, and $\eta$ is an index for denoting $\phi$, $\theta$, $\psi$, $z$, $x$, and $y$. Since such dynamical expressions for $\phi$, $\theta$, $\psi$ have similar formats, we can carry out the analysis only for the variable $\phi$, for the sake of simplicity, and by noting that extensions can be easily performed for the remaining $\theta$ and $\psi$ variables. Also, one can note that the control variable $u_1$ affects states $x, y$, and $z$ at the same time. However, if we consider that the angles $\phi$ and $\theta$ are sufficiently small during the flight, then $u_1$ can be designed thinking about acting on the variable $z$ since $f_z(\mathcal{X}) = F_z \approx 1/m$. Therefore, let us define the error variables as

$$e_\phi \coloneqq \left(\frac{1}{\gamma}\right)\left[(\phi^* - \phi) + e_{\phi 1} + e_{\phi 2}\right] \tag{26}$$

$$e_z \coloneqq \left(\frac{1}{\gamma}\right)\left[(z - z^*) + e_{z1} + e_{z2}\right] \tag{27}$$

in which $\alpha > 0$ is a design constant, $\phi^*$ and $z^*$ are the reference trajectories for states $\phi$ and $z$, respectively, and $e_{\phi 1}$, $e_{\phi 2}$, $e_{z1}$, and $e_{z2}$ are the filtered versions of $e_\phi$ and $e_z$, respectively, defined by

$$\dot{e}_{\phi 1} = -a_1 e_{\phi 1} - b_1 e_\phi \tag{28}$$

$$\dot{e}_{\phi 2} = -a_2 e_{\phi 2} + b_2 e_{\phi 1} \tag{29}$$

$$\dot{e}_{z1} = -a_1 e_{z1} - b_1 e_z \tag{30}$$

$$\dot{e}_{z2} = -a_2 e_{z2} + b_2 e_{z1}. \tag{31}$$

In (28)–(31), $a_1, a_2 > 0$, and $b_1$, $b_2$ are non null constants. After differentiating (26) and (27) two times, we obtain

$$\gamma \ddot{e}_\phi + b_1 \ddot{e}_\phi + b_1(b_2 - a_1)e_\phi = \ddot{\phi}^* - f_\phi(\mathcal{X}) - k_\phi u_2 + K_1 e_{\phi 1} + K_2 e_{\phi 2} \tag{32}$$

$$\gamma \ddot{e}_z + b_1 \ddot{e}_z + b_1(b_2 - a_1)e_z = g - F_z u_1 - \dddot{z}^* + K_1 e_{z1} + K_2 e_{z2} \tag{33}$$

where the constants $K_1$ and $K_2$ have emerged from the combinations of filter parameters $a_1$, $b_1$, $a_2$, and $b_2$. By comparing the left-hand sides of (32) and (33) with the time derivative expression of the sliding surface $\sigma$ in (22), one can note that they are quite identical. Indeed, it is not difficult to demonstrate by back substitution that it is always possible to choose the filter parameters $a_1$, $b_1$, $a_2$, and $b_2$ to match the other surface parameters $\alpha$ and $\beta$. Thus, based on (21) and (22), we can rewrite (32) and (33) to obtain

$$\dot{\sigma}_\phi = -\underbrace{\kappa_\phi k_\phi}_{\rho_\phi} \tanh(\sigma_\phi) \underbrace{-\ddot{\phi}^* - f_\phi(\mathcal{X}) + K_1 e_{\phi 1} + K_2 e_{\phi 2}}_{\mu_\phi} \tag{34}$$

$$\dot{\sigma}_z = -\underbrace{\kappa_z F_z}_{\rho_z} \tanh(\sigma_z) \underbrace{+g - \dddot{z}^* + K_1 e_{z1} + K_2 e_{z2}}_{\mu_z}. \tag{35}$$

To analyze the stability of the error systems $\sigma_\phi$ and $\sigma_z$, the following Lyapunov function candidates are proposed

$$V_1 = \frac{\sigma_\phi^2}{2}, \qquad V_2 = \frac{\sigma_z^2}{2}. \tag{36}$$

After differentiating both $V_1$ and $V_2$ along the trajectories of (34) and (35), we obtain

$$\dot{V}_1 = -|\sigma_\phi| \left[\rho_\phi |\tanh(\sigma_\phi)| + \mu_\phi \text{sign}(\sigma_\phi)\right] \tag{37}$$

$$\dot{V}_2 = -|\sigma_z| \left[\rho_z |\tanh(\sigma_z)| + \mu_z \text{sign}(\sigma_z)\right] \tag{38}$$

from which we can establish the limits of the boundary layer regions that enclose $\sigma_\phi, \sigma_z$

$$\rho_\phi \ |\tanh(\sigma_\phi)| > |\mu_\phi|, \quad \rho_z \ |\tanh(\sigma_z)| > |\mu_z|. \tag{39}$$

Note that the expressions in (39) have identical formats as the one defined in (13), as expected. From (39), it is also possible to verify that outside such regions the magnitudes of both errors decrease because $\dot{V}_1 < 0$ and $\dot{V}_2 < 0$. Since $\rho\tanh(\sigma)$ can be approximated by $\rho\sigma$ around the origin, then for errors sufficiently close to the origin, we can write

$$\rho_\phi |\sigma_\phi| > |\mu_\phi|, \qquad \rho_z |\sigma_z| > |\mu_z|. \tag{40}$$

Thus, from (22) and (39), and after some developments, we can write

$$\ddot{e}_z + \underbrace{\left(\frac{\alpha}{\gamma}\right)}_{\bar{\alpha}} \dot{e}_z + \underbrace{\left(\frac{\beta}{\gamma}\right)}_{\bar{\beta}} e_z = \underbrace{\left(\frac{1}{\gamma}\right)}_{\bar{\gamma}} \dot{\sigma}_z$$

$$e_z = \underbrace{\left(\frac{\bar{\gamma} s}{s^2 + \bar{\alpha} s + \bar{\beta}}\right)}_{M(s)} \sigma_z$$

$$||e_z||_\infty \ \leq \ |M(s)|||\sigma_z||_\infty \tag{41}$$

which corresponds to the steady-state upper bound for $e_z$.

By analyzing the behavior of $\dot{V}_2$ at the boundary layer frontier, i.e., $\rho_z|\sigma_z| = |\mu_z|$, we conclude that $\dot{V}_2 \leq 0$, which still guarantees stability and boundedness for $\sigma_z$. Then, by replacing the last condition into (41), we can state the following upper bound for the output error $e_z$, in steady-state:

$$||e_z||_\infty \ \leq \ \frac{1}{\rho_z}|M(s)|||\mu_z||_\infty. \tag{42}$$

Only for analysis purposes, the magnitude curve of the frequency response of function $M(s)$ is depicted in Fig. 6. Since it is an illustrative plot, the curve is drawn by using the parameters $\bar{\gamma} = 1/10$ and poles lying at $s = -10$, resulting in $\bar{\alpha} = 20$ and $\bar{\beta} = 100$. In this situation, the largest value that $|M(s)|$ can assume over frequency, in linear scale, is $\approx 5.0 \times 10^{-3}$. Thus, since $\bar{\gamma} = 1/\gamma$ and $1/\rho_z = 1/(\kappa_z F_z)$, then the upper bound limit of (42) for $e_z$ in steady-state, can be reduced even more if the design parameters $\gamma$ and $\kappa_z$ are conveniently chosen. It is worth mentioning that large values, in modulus, may result in sufficiently small-size convergence regions together with fast convergence responses.

By extension, the same conclusion can be stated for the upper bound limit for $e_\phi$, namely

$$||e_\phi||_\infty \ \leq \ \frac{1}{\rho_\phi}|M(s)|||\mu_\phi||_\infty \tag{43}$$

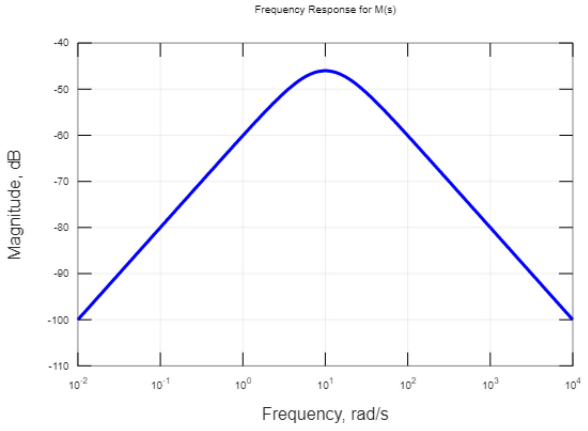


Fig. 6. Frequency response analysis. Magnitude curve of $M(s)$.


Fig. 7. Quadrotor used in the Gazebo software.

but, in this case, also regarding the design parameter $\kappa_\phi$. Such stability and convergence analysis can be carried out on the remaining system's states, thus revealing similar results of steady-state behavior.

## V. Results and Discussion

In this section, we discuss the results obtained with simulations of the proposed controller. The simulation environment and the controller implementation are also presented. Comparisons are made with the original PID controller of the PX4 Firmware.

### A. Simulation Environment

In order to evaluate the proposed strategy safely, this work used the Gazebo software to simulate the test environment. The ROS interface with UAV works as follows. The computer receives the information from a telemetry module available on both the computer and the UAV, using the MAVLink communication protocol. The PX4 software, which runs on the PixHawk flight controller hardware, is responsible for acquiring information from the peripheral sensors and modifying these values in the actuators to which it has access. The GCS runs the operating system Ubuntu 20.04.5 LTS 64 bits with an Intel Core i7-5500U CPU 2.40 GHz × 4, Intel HD Graphics 5500 (Broadwell GT2) with 15.6-GB RAM.

The UAV used in the experiments (3DR iris model) and the world created to simulate the cargo transport between vessels are shown in Figs. 7 and 8, respectively.

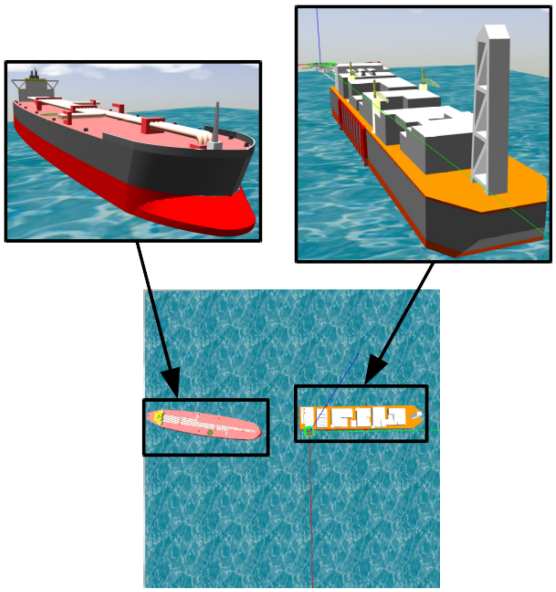

Fig. 8. World created in the Gazebo software.

TABLE II
PID PARAMETERS

| Parameter | $\phi$ | $\theta$ | $\psi$ |
|---|---|---|---|
| P | 0.15 | 0.15 | 0.20 |
| I | 0.20 | 0.20 | 0.10 |
| D | 0.03 | 0.03 | 0.00 |

TABLE III
SMC PARAMETERS

| Parameter | $\phi$ | $\theta$ | $\psi$ |
|---|---|---|---|
| $\kappa$ | 0.26 | 0.26 | 0.08 |
| $\alpha$ | 1 | 1 | 1.20 |
| $\beta$ | 0.2 | 0.2 | 0.10 |
| $\gamma$ | 0.006 | 0.006 | 0.00 |

After carrying out the code modifications on the PX4, it is important to compare the UAV performance using the original PID controller and the modified one with SMC. The PID gains used in the tests, for comparison purposes, are shown in Table II. The parameters for the SMC controller (21) used in these tests can be found in Table III. Note that the PID values are the default ones already implemented in the PX4. In this sense, no modification was necessary. However, a set of values were tested for the SMC until an optimized solution was obtained.

The tests were conducted in three stages, as shown in Fig. 9. In the first stage, the UAV takes off from the original vessel. Then, in the second stage, it approaches the destination vessel by using the autonomous trajectory algorithm. Finally, when reaching the limited distance, it starts to land, which is the end of the third stage.

These stages were performed using the proposed SMC and the original PID algorithms on the internal rate control module of the PX4. State estimation is obtained from the FCU data. Note that the proposed SMC solution and the classical PID control were applied to the system for comparison purposes in the absence and presence of disturbances (i.e., wind).

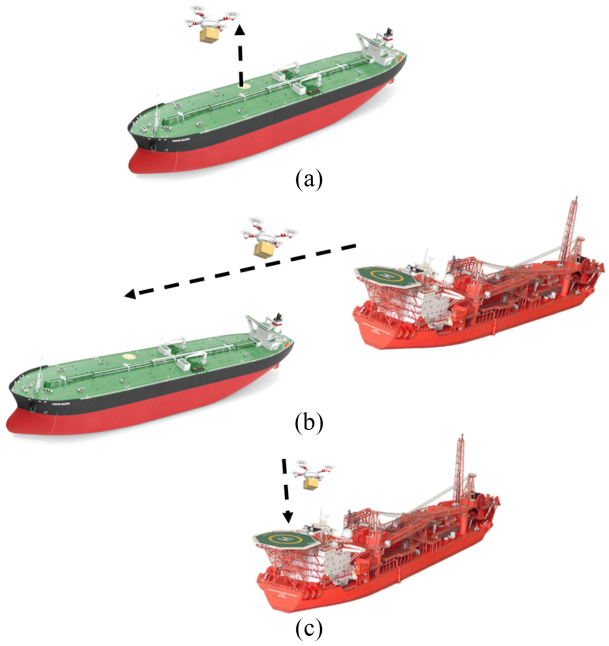


Fig. 9. Tests were conducted in three stages. (a) Take off. (b) Approaching the destination vessel. (c) Landing.

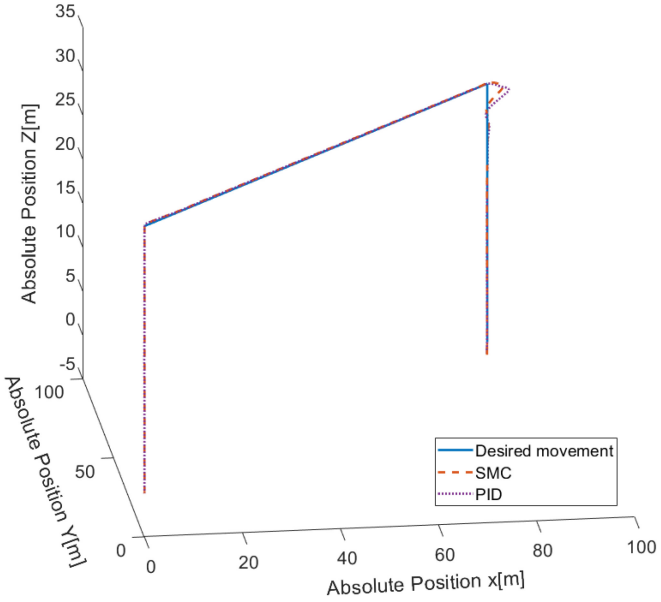


Fig. 10. 3-D visualization of the position reference tracking comparing the SMC and PID controllers considering no external disturbance in the simulation.

*1) Simulation Results Considering the Absence of External Disturbances:* Regarding the proposed scenario of marine small cargo transport, which comprises take off, movement along a trajectory, and then landing, the first set of results presents a comparative performance analysis between the classical PID controller and the SMC strategy for position control along the $x$-, $y$-, and $z$-axis of all three stages.

Fig. 10 gives the outcome for the entire 3-D path performed by both controllers without considering wind in the scenario of going from one ship to another.

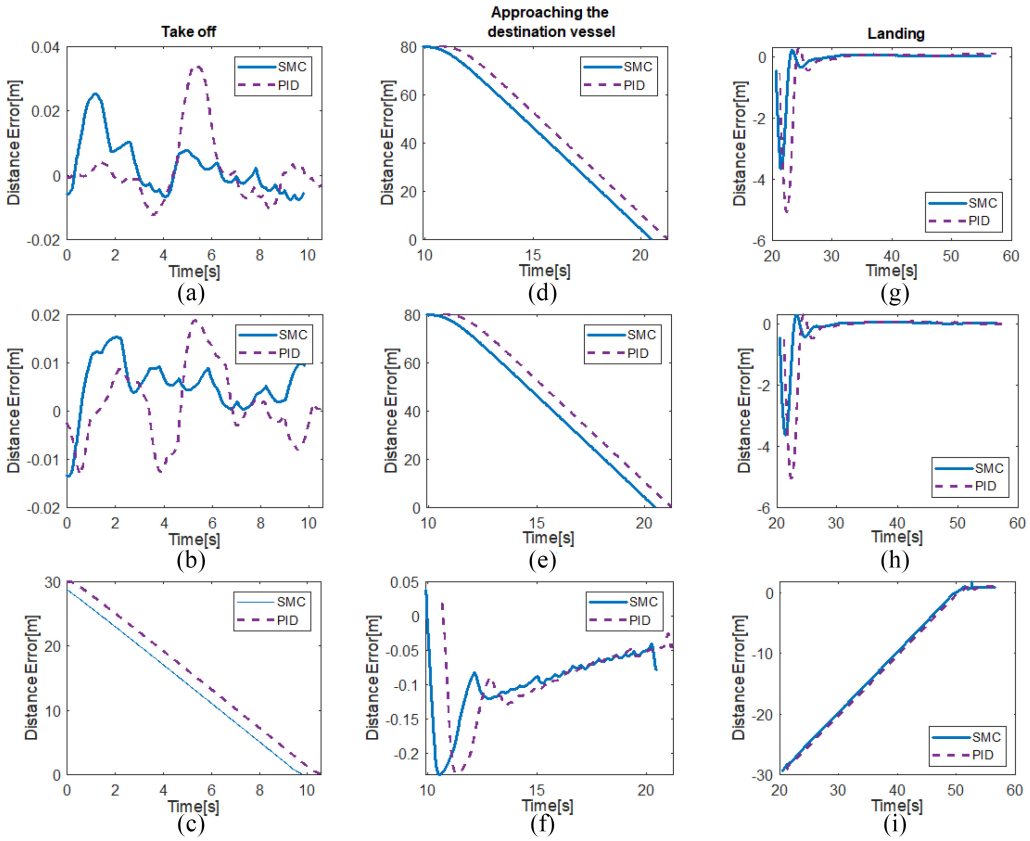


Fig. 11. Position error without disturbances for (a), (d), and (g) *x*-axis, (b), (e), and (h) *y*-axis, and (c), (f), and (i) *z*-axis.

As expected, when achieving desired maneuvers, the SMC performs satisfactorily similar to the one obtained with the PID. That is, both controllers were capable of tracking the desired position with negligible steady-state errors, demonstrating fewer performance differences in the case of the absence of external disturbances.

The results for the positioning error in the *x*-, *y*-, and *z*-axis of the three stages are shown, respectively, in Fig. 11. This is the same test case as the former results in Fig. 10, in which no external disturbances such as wind current and/or variable mass cargo exist.

Note that on takeoff and landing tasks, the results in the *z*-axis are not comparable as they seem almost identical, and the same occurs on the *x*- and *y*-axis while moving between ships. That happens because these axes are subjected to the largest changes in the desired position along the step.

It is possible to observe that the proposed SMC strategy behaves similarly to the classical PID available for the PX4 firmware under these conditions. However, using the SMC controller can also verify that some disturbances are compensated better. Small overshoots on the *x*- and *y*-axis are observed in the landing phase right after they reach their targets when moving from one ship to another.

*2) Simulation Results Considering the Presence of External Disturbances:* Fig. 12 shows the entire 3-D path for the position reference tracking to observe both controllers' behavior when dealing with external disturbances. Note that

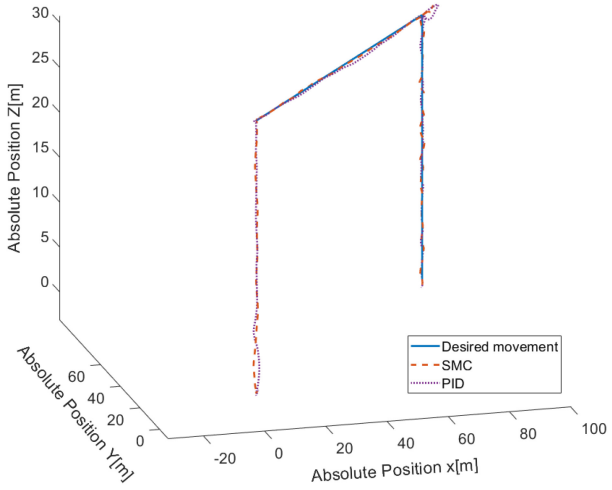


Fig. 12. 3-D visualization for comparing the SMC and PID controllers for position control considering wind.

in applications in real scenarios, UAVs can suffer from environmental disturbances. such as wind, magnetic fields, or uncertain disturbance effects (i.e., sensor noise or payload). Thus, aerial systems must have a robust control for attitude and stabilization problems [62], [63].

To demonstrate the effectiveness and robustness of the SMC controller, this simulation considers the same wind current in both simulation trials. Note that the SMC performed better than the classical PID in tracking the reference inputs.

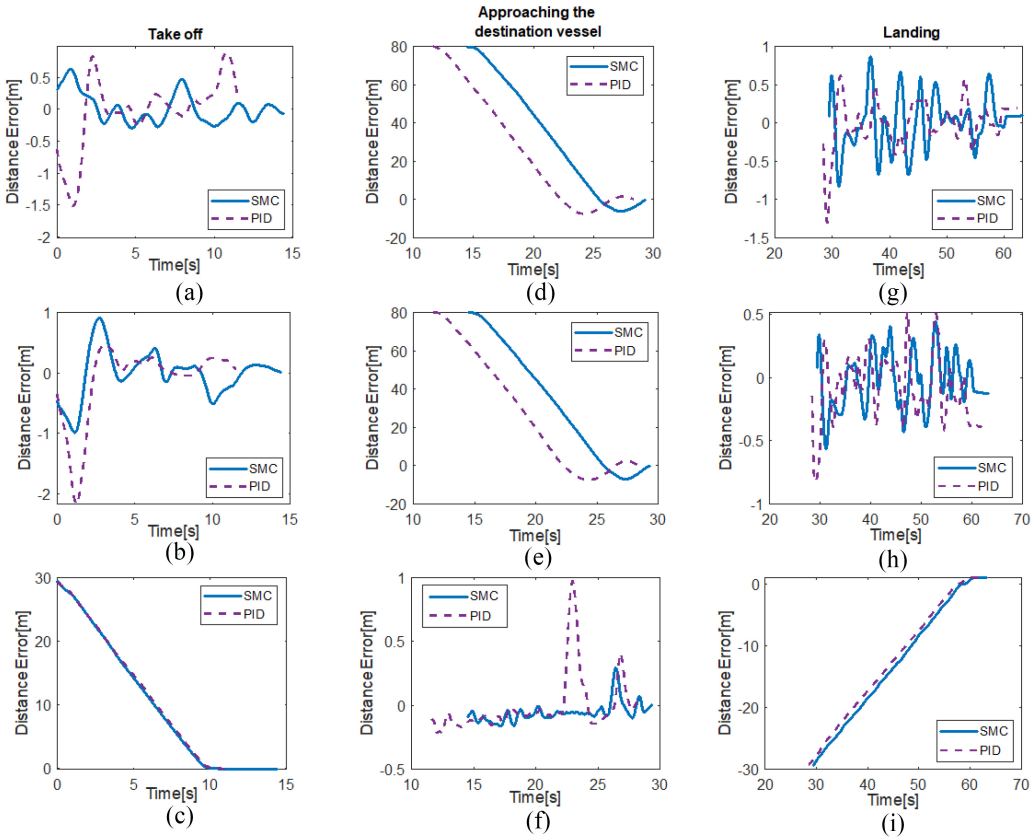


Fig. 13. Position error with disturbances for (a), (d), and (g) *x*-axis, (b), (e), and (h) *y*-axis, and (c), (f), and (i) *z*-axis.

Fig. 13 gives the position errors of both controllers along the *x*-, *y*-, and *z*-axis, for all three stages of the proposed scenario, respectively. Note that the output obtained with SMC has less oscillatory behavior around the reference value than that obtained with the PID. The SMC also presented even better performance under disturbance circumstances in terms of the convergence velocity of the tracking error. Thus, this kind of result can help to understand the importance of the implementation of this robust controller into the PX4 hardware.

In the initial takeoff step, there is a gust of wind that the SMC counteracts better. There is also an upward gust on the movement step that almost does not interfere with the quadcopter when the rate controller is under the SMC algorithm.

One point that is valid to mention is that the path controller algorithm of the WPG package considers that the UAV arrives at the destination if the distance from the current point to the desired point is less than 0.1 m in all directions. Basically, inside a cube (side of 20 cm) centered on the desired point. And only when that happens does the WPG package send the drone to the next desired destination. So, the algorithm that does the path in less time in an environment with high disturbances is not necessarily the better, as one could reach by chance the "checkpoint area" faster.

In order to define the best controller in this situation, we need to observe the maximum average error (MAE) that both present. The PID has an MAE of 0.35 m, and the SMC controller with the PID surface has an MAE of 0.16 m.

Note that the trajectory tracking performance demonstrated the effectiveness of the SMC solution embedded in a PX4 FCU against the adverse condition, as expected from theoretical analysis. The outcomes obtained by this work reaffirm the good performance of the SMC directly implemented in the firmware of the PX4 and its capacity for disturbance rejection, as previously mentioned in the works of [37], [41], [44], and [42]. It is not easy to compare the proposed solution with these mentioned ones due to the necessity of inserting all of them in the PX4 firmware to perform the software-in-the-loop (SITL) tests. Besides, all these mentioned works were evaluated using numerical simulation.

Another comparison can be performed regarding the SMC proposed in this scenario and other advanced control methods such as model predictive control (MPC) [64] and reinforcement learning (RL) [65]. The SMC provides a simpler and more straightforward implementation than MPC, as it does not require formulating an optimization problem or relying on a dynamic system model. This simplicity allows for easier parameter tuning and reduces computational complexity. Besides, SMC excels in handling uncertainties and disturbances, making it robust in real-world scenarios where the precise model of the UAV might not be available or may change over time. On the other hand, the RL requires extensive training and may struggle with convergence issues or the need for a large amount of data. Additionally, human operators can more easily interpret and understand SMC, facilitating system diagnosis and troubleshooting. In this sense,

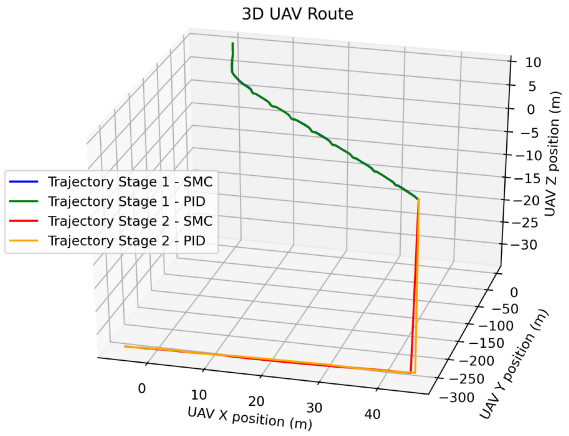


Fig. 14. 3-D visualization for comparing the SMC and PID controllers in autonomous trajectory simulation.

SMC demonstrates the advantages of simplicity, robustness, and interpretability, making it a suitable control strategy for the proposed scenario compared to more complex and data-intensive methods like MPC and RL. In contrast, the Slide Mode Controller (SMC) offers a simpler implementation that does not require a precise model, making it more suitable for real-world scenarios. Besides, SMC can be directly integrated into the PX4 system without extensive modifications, leveraging the simplicity of PID controllers.

### B. Autonomous Trajectory Results

These simulations were conducted under the same environment, one using the classic PX4 PID controller and one using the implemented SMC. The objective was to verify if the implemented SMC responds better when the UAV is carrying cargo subjected to offshore environmental conditions. The simulations can be observed in the video recording available at [66]. Fig. 14 presents the simulation results.

When compared to the ideal trajectory, the PID has an MAE of 0.35 m, and the SMC controller with the PID surface has an MAE of 0.16 m. As presented before, the initial trajectory is performed with the UAV following geospatial waypoints, so both controllers execute almost the same course in this trajectory.

The major difference was in stage 2, where the UAV navigates toward the marker of the final destination with the trajectory corrected by an EKF sensor fusion between the camera data and the avionic positioning and attitude data. In this stage, the SMC had fewer errors than PID. The SMC also provides a quicker operation than the PID, finding the marker within 2 min 48 s, while the PID took 3 min 34 s, probably by being more stable and, therefore, the camera input for the OpenCV in smoother. Therefore, the implemented SMC controller is an advanced option for flight robustness for operations in harsh environments like the one proposed in this work.

The simulations show good results when applying the proposed methodology in real-life missions. For example, from Figs. 10 and 12, it is possible to verify that the UAV was able to deliver the cargo at 100 m from the deployment point, being able to improve such distance even more. In a real offloading operation presented in [14], this could easily replace the pneumatic line thrower (PLT) to complete the mooring process or deliver fluid samples between vessels. This is also an improvement from the PLT, which makes the approaching between vessels mandatory and has several restrictions when the two vessels that must send and receive parcels or towlines have relative movement, as reported in [67].

Also from this SITL simulation test, it is possible to verify that the proposed strategy offers advantages, such as enhanced stability, simplified parameter tuning, and autonomous offshore cargo capabilities for UAVs. Integrating an SMC into the PX4 FCU improves stability and robustness against external disturbances. Besides, by combining the SMC with computer vision techniques and sensor data fusion, the control strategy enabled the UAV to autonomously perform the proposed offshore cargo tasks in the context of Oil & Gas industry. However, limitations in this proposition include the need for real-world validation, complex integration requirements, and considerations of scalability and adaptability. Therefore, further research and experimentation are needed to ensure the practical implementation of the proposed control strategy.

## VI. Conclusion and Future Works

The PID controller has been widely used in the literature and industry due to its simple structure. However, this controller adjustment can be difficult in practical terms. Regarding UAVs, external disturbances, such as wind, actuator failure, and parametric uncertainties, can cause physical instability of the UAV's platform. UAVs commonly use a classical PID controller. A drawback is the necessity of expertise from the operator to adjust the parameters to deal with nonlinearities.

This work developed and implemented an SMC controller in a PX4 FCU software for a quadrotor UAV and a computer vision technique to apply an autonomous UAV in an offshore cargo task for the Oil and Gas sector. Experimental tests were conducted in a realistic simulation environment using ROS and Gazebo platforms to verify the performances of the methodology. The results demonstrated the robustness of the SMC implemented in the PX4 FCU software. This work opens the possibility of several improvements in terms of implementation. In future works, the authors intend to carry out the same test performed in the Gazebo software simulation in which the quadrotor moves between ships carrying a cargo transport.

## Acknowledgment

The authors have no conflicts of interest to declare that are relevant to the content of this article. They also would like to thank the following federal Brazilian agencies, CEFET-RJ, CAPES, CNPq, and FAPERJ, for supporting this work.

## References

[1] A. G. Melo, M. F. Pinto, L. M. Honorio, F. M. Dias, and J. E. N. Masson, "3D correspondence and point projection method for structures deformation analysis," *IEEE Access*, vol. 8, pp. 177823–177836, 2020.

[2] M. F. Pinto, L. M. Honorio, A. Melo, and A. L. M. Marcato, "A robotic cognitive architecture for slope and dam inspections," *Sensors*, vol. 20, no. 16, p. 4579, 2020.

[3] M. F. Pinto et al., "ARCog: An aerial robotics cognitive architecture," *Robotica*, vol. 39, no. 3, pp. 483–502, 2021.

[4] C. C. Murray and R. Raj, "The multiple flying sidekicks traveling salesman problem: Parcel delivery with multiple drones," *Transp. Res. C, Emerg. Technol.*, vol. 110, pp. 368–398, Jan. 2020.

[5] Á. Madridano, A. Al-Kaff, D. Martín, and A. de la Escalera, "3D trajectory planning method for UAVs swarm in building emergencies," *Sensors*, vol. 20, no. 3, p. 642, 2020.

[6] M. F. Pinto, A. G. Melo, A. L. M. Marcato, and C. Urdiales, "Case-based reasoning approach applied to surveillance system using an autonomous unmanned aerial vehicle," in *Proc. IEEE 26th Int. Symp. Ind. Electron. (ISIE)*, 2017, pp. 1324–1329.

[7] M. F. Pinto, F. O. Coelho, J. P. C. De Souza, A. G. Melo, A. L. M. Marcato, and C. Urdiales, "EKF design for online trajectory prediction of a moving object detected onboard of a UAV," in *Proc. 13th APCA Int. Conf. Automat. Control Soft Comput. (CONTROLO)*, 2018, pp. 407–412.

[8] A. G. Melo, M. F. Pinto, A. L. M. Marcato, L. M. Honório, and F. O. Coelho, "Dynamic optimization and heuristics based online coverage path planning in 3D environment for UAVs," *Sensors*, vol. 21, no. 4, p. 1108, 2021.

[9] S. Stavinoha, H. Chen, M. Walker, B. Zhang, and T. Fuhlbrigge, "Challenges of robotics and automation in offshore oil&gas industry," in *Proc. 4th Annu. IEEE Int. Conf. Cyber Technol. Autom. Control Intell.*, 2014, pp. 557–562.

[10] F. A. A. Andrade et al., "Unmanned aerial vehicles motion control with fuzzy tuning of cascaded-PID gains," *Machines*, vol. 10, no. 1, p. 12, 2022.

[11] F. Wen, J. Wolling, K. McSweeney, and H. Gu, "Unmanned aerial vehicles for survey of marine and offshore structures: A classification organization's viewpoint and experience," presented at the Offshore Technol. Conf., Houston, TX, USA, 2018.

[12] G. S. Ramos, M. F. Pinto, F. O. Coelho, L. M. Honório, and D. B. Haddad, "Hybrid methodology based on computational vision and sensor fusion for assisting autonomous UAV on offshore messenger cable transfer operation," *Robotica*, vol. 40, no. 8, pp. 2786–2814, 2022.

[13] T. R. Wanasinghe, R. G. Gosine, O. De Silva, G. K. I. Mann, L. A. James, and P. Warrian, "Unmanned aerial systems for the oil and gas industry: Overview, applications, and challenges," *IEEE Access*, vol. 8, pp. 166980–166997, 2020.

[14] G. S. Ramos, M. F. Pinto, E. S. S. de Souza, G. B. Machado, and G. G. R. de Castro, "Technical and economic feasibility study for implementing a novel mooring-assisting methodology in offloading operations using autonomous unmanned aerial vehicles," *SPE Prod. Oper.*, vol. 37, no. 1, pp. 72–87, 2022.

[15] Y. Dai, B. Lin, Y. Che, and L. Lyu, "UAV-assisted data offloading for smart container in offshore maritime communications," *China Commun.*, vol. 19, no. 1, pp. 153–165, Jan. 2022.

[16] S. Asadzadeh, W. J. de Oliveira, and C. R. de Souza Filho, "UAV-based remote sensing for the petroleum industry and environmental monitoring: State-of-the-art and perspectives," *J. Petrol. Sci. Eng.*, vol. 208, Jan. 2022, Art. no. 109633.

[17] W. H. Maes and K. Steppe, "Perspectives for remote sensing with unmanned aerial vehicles in precision agriculture," *Trends Plant Sci.*, vol. 24, no. 2, pp. 152–164, 2019.

[18] H. Guan et al., "UAV-Lidar aids automatic intelligent powerline inspection," *Int. J. Elect. Power Energy Syst.*, vol. 130, Sep. 2021, Art. no. 106987.

[19] I. Z. Biundini, M. F. Pinto, A. G. Melo, A. L. M. Marcato, L. M. Honório, and M. J. R. Aguiar, "A framework for coverage path planning optimization based on point cloud for structural inspection," *Sensors*, vol. 21, no. 2, p. 570, 2021.

[20] Y. Tan, S. Li, H. Liu, P. Chen, and Z. Zhou, "Automatic inspection data collection of building surface based on BIM and UAV," *Autom. Constr.*, vol. 131, Nov. 2021, Art. no. 103881.

[21] P. H. Nguyen, M. Arsalan, J. H. Koo, R. A. Naqvi, N. Q. Truong, and K. R. Park, "LightDenseYOLO: A fast and accurate marker tracker for autonomous UAV landing by visible light camera sensor on drone," *Sensors*, vol. 18, no. 6, p. 1703, 2018.

[22] D. J. Almakhles, "Robust backstepping sliding mode control for a quadrotor trajectory tracking application," *IEEE Access*, vol. 8, pp. 5515–5525, 2019.

[23] H. L. N. N. Thanh and S. K. Hong, "Quadcopter robust adaptive second order sliding mode control based on PID sliding surface," *IEEE Access*, vol. 6, pp. 66850–66860, 2018.

[24] K. Eltag, M. S. Aslamx, and R. Ullah, "Dynamic stability enhancement using fuzzy PID control technology for power system," *Int. J. Control Autom. Syst.*, vol. 17, no. 1, pp. 234–242, 2019.

[25] X. Hu and J. Liu, "Research on UAV balance control based on expert-fuzzy adaptive PID," in *Proc. IEEE Int. Conf. Adv. Elect. Eng. Comput. Appl. (AEECA)*, 2020, pp. 787–789.

[26] D. Lee, H. J. Kim, and S. Sastry, "Feedback linearization vs. adaptive sliding mode control for a quadrotor helicopter," *Int. J. Control Autom. Syst.*, vol. 7, no. 3, pp. 419–428, 2009.

[27] L. Martins, C. Cardeira, and P. Oliveira, "Feedback linearization with zero dynamics stabilization for quadrotor control," *J. Intell. Robot. Syst.*, vol. 101, no. 1, pp. 1–17, 2021.

[28] A. Das, K. Subbarao, and F. Lewis, "Dynamic inversion with zero-dynamics stabilisation for quadrotor control," *IET Control Theory Appl.*, vol. 3, no. 3, pp. 303–314, 2009.

[29] U. Ansari and A. H. Bajodah, "Robust generalized dynamic inversion quadrotor control," *IFAC-PapersOnLine*, vol. 50, no. 1, pp. 8181–8188, 2017.

[30] R. Xu and U. Ozguner, "Sliding mode control of a quadrotor helicopter," in *Proc. 45th IEEE Conf. Decis. Control*, 2006, pp. 4957–4962.

[31] N. Ahmed and M. Chen, "Sliding mode control for quadrotor with disturbance observer," *Adv. Mech. Eng.*, vol. 10, no. 7, 2018, Art. no. 1687814018782330.

[32] A. Das, F. Lewis, and K. Subbarao, "Backstepping approach for controlling a quadrotor using Lagrange form dynamics," *J. Intell. Robot. Syst.*, vol. 56, no. 1, pp. 127–151, 2009.

[33] X. Huo, M. Huo, and H. R. Karimi, "Attitude stabilization control of a quadrotor UAV by using backstepping approach," *Math. Problems Eng.*, vol. 2014, Feb. 2014, Art. no. 749803.

[34] "An in-depth look at the multicopter control system architecture." P D Community Writers. 2020. Accessed: Mar. 2, 2022. [Online]. Available: https://sched.co/cjOm

[35] M. K. Joyo, D. Hazry, S. F. Ahmed, M. H. Tanveer, F. A. Warsi, and A. T. Hussain, "Altitude and horizontal motion control of quadrotor UAV in the presence of air turbulence," in *Proc. IEEE Conf. Syst. Process Control (ICSPC)*, 2013, pp. 16–20.

[36] G. Carvalho et al., "Hybrid PID-fuzzy controller for autonomous UAV stabilization," in *Proc. 14th IEEE Int. Conf. Ind. Appl. (INDUSCON)*, 2021, pp. 1296–1302.

[37] N. P. Nguyen, N. X. Mung, H. L. N. N. Thanh, T. T. Huynh, N. T. Lam, and S. K. Hong, "Adaptive sliding mode control for attitude and altitude system of a quadcopter UAV via neural network," *IEEE Access*, vol. 9, pp. 40076–40085, 2021.

[38] A. Benallegue, A. Mokhtari, and L. Fridman, "High-order sliding-mode observer for a quadrotor UAV," *Int. J. Robust Nonlinear Control IFAC-Affiliated J.*, vol. 18, nos. 4–5, pp. 427–440, 2008.

[39] S. Mobayen, "Design of CNF-based nonlinear integral sliding surface for matched uncertain linear systems with multiple state-delays," *Nonlinear Dyn.*, vol. 77, no. 3, pp. 1047–1054, 2014.

[40] F. Chen, R. Jiang, K. Zhang, B. Jiang, and G. Tao, "Robust backstepping sliding-mode control and observer-based fault estimation for a quadrotor UAV," *IEEE Trans. Ind. Electron.*, vol. 63, no. 8, pp. 5044–5056, Aug. 2016.

[41] O. Mofid and S. Mobayen, "Adaptive sliding mode control for finite-time stability of quad-rotor UAVs with parametric uncertainties," *ISA Trans.*, vol. 72, pp. 1–14, Jan. 2018.

[42] W. Cai, J. She, M. Wu, and Y. Ohyama, "Disturbance suppression for quadrotor UAV using sliding-mode-observer-based equivalent-input-disturbance approach," *ISA Trans.*, vol. 92, pp. 286–297, Sep. 2019.

[43] G. E. M. Abro, S. A. B. M. Zulkifli, V. S. Asirvadam, and Z. A. Ali, "Model-free-based single-dimension fuzzy SMC design for underactuated quadrotor UAV," *Actuators*, vol. 10, p. 191, Aug. 2021.

[44] H. Ríos, J. González-Sierra, and A. Dzul, "Robust tracking output-control for a quad-rotor: A continuous sliding-mode approach," *J. Franklin Inst.*, vol. 354, no. 15, pp. 6672–6691, 2017.

[45] J.-J. E. Slotine and W. Li, *Applied Nonlinear Control*. Englewood Cliffs, NJ, USA: Prentice-Hall, 1991.

[46] K. A. Alattas et al., "Barrier function adaptive nonsingular terminal sliding mode control approach for quad-rotor unmanned aerial vehicles," *Sensors*, vol. 22, no. 3, p. 909, 2022.

[47] A. Gupta, T. Afrin, E. Scully, and N. Yodo, "Advances of UAVs toward future transportation: The state-of-the-art, challenges, and opportunities," *Future Transp.*, vol. 1, no. 2, pp. 326–350, 2021.

[48] R. Kellermann, T. Biehle, and L. Fischer, "Drones for parcel and passenger transportation: A literature review," *Transp. Res. Interdiscipl. Perspect.*, vol. 4, Mar. 2020, Art. no. 100088.

[49] J. R. Scalea et al., "Successful implementation of unmanned aircraft use for delivery of a human organ for transplantation," *Ann. Surg.*, vol. 274, no. 3, pp. e282–e288, 2021.

[50] Y. R. Petillot, G. Antonelli, G. Casalino, and F. Ferreira, "Underwater robots: From remotely operated vehicles to intervention-autonomous underwater vehicles," *IEEE Robot. Autom. Mag.*, vol. 26, no. 2, pp. 94–101, Jun. 2019.

[51] "Tugboat company takes its business flying with drones." Society of Petroleum Engineers. 2018. Accessed: Jun. 15, 2020. [Online]. Available: https://jpt.spe.org/tugboat-company-takes-its-business-flying-drones

[52] P. Durdevic, D. Ortiz-Arroyo, S. Li, and Z. Yang, "Vision aided navigation of a quad-rotor for autonomous wind-farm inspection," *IFAC-PapersOnLine*, vol. 52, no. 8, pp. 61–66, 2019.

[53] L. Qingqing et al., "Towards active vision with UAVs in marine search and rescue: Analyzing human detection at variable altitudes," in *Proc. IEEE Int. Symp. Safety Secur. Rescue Robot. (SSRR)*, 2020, pp. 65–70.

[54] M. Hlas and J. Straub, "Autonomous navigation and control of unmanned aerial systems in the national airspace," in *Proc. IEEE Aerosp. Conf.*, 2016, pp. 1–7.

[55] A. Faust, I. Palunko, P. Cruz, R. Fierro, and L. Tapia, "Automated aerial suspended Cargo delivery through reinforcement learning," *Artif. Intell.*, vol. 247, pp. 381–398, Jun. 2017.

[56] M. Lieret, V. Kogan, S. Döll, and J. Franke, "Automated in-house transportation of small load carriers with autonomous unmanned aerial vehicles," in *Proc. IEEE 15th Int. Conf. Autom. Sci. Eng. (CASE)*, 2019, pp. 1010–1015.

[57] M. Castillo-Effen, C. Castillo, W. Moreno, and K. Valavanis, "Control fundamentals of small / miniature helicopters—A survey," in *Advances in Unmanned Aerial Vehicles*. Dordrecht, The Netherlands: Springer, 2007, pp. 73–118.

[58] G. Hoffmann, H. Huang, S. Waslander, and C. Tomlin, "Quadrotor helicopter flight dynamics and control: Theory and experiment," in *Proc. AIAA Guid. Navig. Control Conf. Exhibit*, 2007, p. 6461.

[59] P.-J. Bristeau, P. Martin, E. Salaün, and N. Petit, "The role of propeller aerodynamics in the model of a quadrotor UAV," in *Proc. Eur. Control Conf. (ECC)*, 2009, pp. 683–688.

[60] C. Karney and R. Deakin, "F.W. Bessel (1825): The calculation of longitude and latitude from geodesic measurements," *Astron. Notes*, vol. 331, no. 8, pp. 852–861, 2010.

[61] "PX4 system architecture documentation." P D Community Writers. 2022. Accessed: Apr. 2, 2021. [Online]. Available: https://docs.px4.io/master/en/concept/px4_systems_architecture.html

[62] C. Sun, M. Liu, C. Liu, X. Feng, and H. Wu, "An industrial quadrotor UAV control method based on fuzzy adaptive linear active disturbance rejection control," *Electronics*, vol. 10, no. 4, p. 376, 2021.

[63] Ş. Ulus and I. Eski, "Neural network and fuzzy logic-based hybrid attitude controller designs of a fixed-wing UAV," *Neural Comput. Appl.*, vol. 33, no. 14, pp. 8821–8843, 2021.

[64] Y. Zhang, Y. Zhang, and Z. Yu, "Path following control for UAV using deep reinforcement learning approach," *Guid. Navig. Control*, vol. 1, no. 1, 2021, Art. no. 2150005.

[65] B. Jiang, B. Li, W. Zhou, L.-Y. Lo, C.-K. Chen, and C.-Y. Wen, "Neural network based model predictive control for a quadrotor UAV," *Aerospace*, vol. 9, no. 8, p. 460, 2022.

[66] *Sliding Mode Controller Applied to Autonomous UAV Operation in Marine Small Cargo Transport*. 2022. Accessed: Nov. 6, 2022. [Online Video]. Available: https://www.youtube.com/watch?v=pdxp2breakYiC6e4

[67] "Tanker Towline deployment bat review: Final report." 2023. Accessed: May 30, 2023. [Online]. Available: glosten.com/Tanker-Towline-BAT-Review.pdf